Journal of Membrane Science 460 (2014) 148–159

Contents lists available at ScienceDirect

Journal of Membrane Science

journal homepage: www.elsevier.com/locate/memsci

Analysis of Donnan-dialyzer irreproducibility and experimental study of a microfluidic parallel-plate membrane-separation module for total analysis systems

Dohyun Kim [a,b,*], Jack W. Judy [a,1]

[a] Electrical Engineering Department, University of California, Los Angeles, 420 Westwood Plaza, Los Angeles, CA 90095, United States
[b] Department of Mechanical Engineering, Myongji University, Yongin-si, Gyeonggi-do 449-728, Republic of Korea

ARTICLE INFO

Article history:
Received 7 December 2013
Received in revised form
17 February 2014
Accepted 19 February 2014
Available online 28 February 2014

Keywords:
Membrane separation
Donnan dialysis
Ion-exchange membrane
Parallel-plate dialyzer
Microfluidics

ABSTRACT

We report irreproducibility analysis of miniaturized, batch, continuous stirred-tank Donnan dialyzers (CSDD) designed for a membrane-separation module of chemical analysis systems. Theoretical analysis indicates that a high exchange capacity of ion-exchange membrane (>1 mol L^{-1}) causes a significant irreproducibility of the CSDDs when the dialysate/sample volume is relatively small (<10 mL) and the ionic strength is low (<0.01 M). Numerical simulation based on Nernst–Planck flux equation and Donnan-equilibrium equation shows a significant deviation from the ideal Donnan-dialyzer response, and this irreproducibility is verified with experiments. In order to address the irreproducibility issue, we introduce a novel, microfluidic, parallel-plate Donnan-dialytic membrane-separation module (PDMM) with recirculation tube. The recirculation tube works as a dialysate/sample container as well as an effective mixer. The rationally designed PDMM has advantages over the CSDDs in that (1) the dialysis throughput is improved (6 folds), and (2) the dialysis irreproducibility is reduced (4 folds). Dialysis efficiency of our PDMM is also high (~91%), compared with that of flow-through parallel-plate dialyzers (usually ~1%).

1. Introduction

Since the advent of the first microfabricated gas chromatography on chip [1], the field of microanalytical systems, also referred as lab-on-a-chip or μTAS (micro-total-analysis-systems) has grown tremendously. The microanalytical systems promise to integrate time-consuming, labor-intensive, complicated analytical procedures into a single microinstrument and to revolutionize clinical, chemical, biological, and environmental analyses [2]. Despite some commercial success [3,4], many of novel, creative ideas for microanalytical-system research merely settled with scientific papers. Many believes, at least from the technical point of view, that difficulty of commercialization lies on the lack of effective sample-preparation methods seamlessly incorporated into the μTAS [5,6]. One has to solve "front-end problems": interfacing real-world sample with microfluidic systems, and preparing samples to render them suitable for downstream separation and detection [6].

Among sample-preparation techniques (e.g., separation, preconcentration, derivatization, biological sample treatment) [7,5], the separation is particularly challenging because raw sample matrix usually contains impurities of various sizes spanning nanoscale to microscales that may cause clogging in microfluidic channels and measurement interference [5]. For example, a microfluidic electrochemical nitrate sensor exhibited interference from various ionic species in groundwater [8], and tear proteins caused nonspecific surface fouling and background-signal increase in microfluidic Western blotting [9]. In order to isolate and clean up impurities, strategies implemented in microanalytical systems include solid-phase extraction [10], chelation [11], precipitation [12], differential diffusion between laminar flows [13] and membrane-based separation [14,15].

Dialysis is a well-established, attractive membrane-based separation technique. In general, dialysis is simple, reliable, high-throughput and modular [16]. Dialysis has been adopted for clinical applications [17] and environmental analysis [16,18]. Dialysis has been successfully employed for μTAS [15,19,20] as well. Passive dialysis employed for separation of neutral species has drawbacks: (1) poor dialysis efficiency of theoretically maximum 50% in equilibrium stopped-flow condition or commonly much less ($<1\%$) in a non-equilibrium continuous-flow mode [21], and (2) no permselectivity toward interferents of a similar size but different charges. Active or Donnan dialysis employs ion-exchange membrane for charge and size speciation.

* Corresponding author. Present address: Department of Mechanical Engineering, Myongji University, Yongin-si, Gyeonggi-do 449-728, Republic of Korea.
Tel.: +82 31 324 1425; fax: +82 31 330 6957.
E-mail addresses: dohyun.kim@mju.ac.kr (D. Kim), jack.judy@ufl.edu (J.W. Judy).
[1] Present address is Electrical and Computer Engineering Department, University of Florida, 216 Larsen Hall, Gainesville, FL 32611, United States.

http://dx.doi.org/10.1016/j.memsci.2014.02.029
0376-7388

Donnan dialysis has advantages over electrodialysis as no external electric field is required. Analytes are not altered significantly electrochemically and less energy is consumed. Another excellent analytical aspect of Donnan dialysis is that it can enrich analytes (i.e., preconcentration) [22,23].

The conventional Donnan dialysis is far from being ideal for microanalytical systems. Firstly, dialysis efficiency is low in nonequilibrium continuous-flow mode [24]. Therefore, stopped-flow mode is often employed to improve the efficiency [22]. Solutions should be thoroughly agitated to improve mass transfer in the stopped-flow condition. Secondly, sample and dialysate consumption is large. A simple remedy could be to scale down solution containers to microscale. However, effective agitation in the microscale containers would be particularly challenging [25]. Thirdly, scaling down of physical dimensions of a dialyzer causes an unnotice but critical issue – irreproducibility. The analytes in sample solution are transferred to the dialysate through the membrane. Owing to a high concentration of fixed-ionic groups (i.e., >1 mol L^{-1}) and electroneutrality condition, the membrane acts as a "counterion storage". The stored counterions in high concentration cause the dialysis process to depend on the prior dialysis condition (i.e., irreproducible dialysis). The irreproducibility becomes significant when ionic strength is low and solution volume is small (typical for clinical and environmental samples and/or for microanalytical systems).

In the first part of this communication, the impact of the dialysis condition on the irreproducibility is for the first time, to the best of our knowledge, theoretically and experimentally analyzed. Equilibrium concentrations of ions in dialysate, sample and membrane phases of a Donnan dialyzer are modeled using the Nernst–Planck formulation and the Donnan equilibrium equation. The numerical model is used to predict the dialyzer output in a series of repeated dialysis steps, for three different cases of the dialyzer input (i.e., initial analyte concentrations in sample solution): (1) constant, (2) randomly changing, and (3) monotonically increasing. We also show how the irreproducibility is alleviated by increasing solution-to-membrane volume ratio, a critical dialyzer design parameter. The numerical model is verified by experiments using CSDDs fabricated in house.

There have been efforts to address the aforementioned issues of the conventional Donnan dialyzers for analytical systems. A long tubular ion-exchange membrane was used as a dialysate container and the tube was dipped into an agitated sample solution for analyte recovery under stopped-flow condition [26]. Cox et al. proposed a similar system with the difference being dialysate in flow condition for a high throughput [27], but the dialysis efficiency was low because of nonequilibrium condition. Instead of stirring, forcing solution through a dialyzer at a high flow rate yielded effective agitation and improved throughput [28,29]. A tubular membrane for dialysate solution was enclosed in a tube-like sample container and the sample solution was recirculated in a closed loop. Using the recirculation approach, the dialysis was completed at a reasonable speed [28]. On the other hand, Miliosavljevic et al. recirculated the dialysate solution through a parallel-plate Donnan dialyzer while the sample solution was stationary [30].

In the second part of the communication, we introduce for the first time, to the best of our knowledge, a parallel-plate Donnan-dialytic membrane-separation module (PDMM) with recirculation tubes for both dialysate and sample solutions *that does not require active agitation*. The PDMM is fully automated, and the dialyzer performance (e.g., throughput, reproducibility, dialysis efficiency) is improved over the CSDDs we tested. The novelty of the PDMM lies on a microfluidic parallel-plate dialyzer, recirculation of dialysate/sample solutions through small-bore tubes, and the use of equilibrium dialysis condition. A major difference from work by Velizarov et al. [29] is that (1) they use stirred tanks for agitation and (2) an enzyme bioreactor tank is connected to the recirculation loop for nitrate removal, which renders the system not amenable to a microfluidic/miniaturized format. By rational design, we achieve the following important results: (1) the dialyzer irreproducibility is significantly reduced by increasing the solution-to-membrane-volume ratio; (2) throughput is improved by forced convection in the both recirculation tubes; and (3) dialysis efficiency is much higher ($\sim$91%) than that of a flow-through dialyzer as the PDMM operates in an equilibrium condition. Additionally, the microchannel-based, simple dialyzer design is amenable to on-chip integration of the sample preparation module into microanalytical systems. Toward a total analysis system integrated with membrane sample preparation, dialysis experiments for nitrate, an important environmental analyte [31], are performed using the CSDDs and the PDMM, and the results are compared.

2. Experimental

2.1. Chemical reagents

In preparing reagents, 16 MΩ cm deionized (DI) water from Super-Q Plus High Purity Water System (Millipore, Billerica, MA, USA) was used. All chemicals were ACS reagent grade. Nitrate, chloride, and fluoride concentrations were measured using ion-selective electrodes (ISE) model 360-75, 364-75, and 365-75, respectively (SENTEK Limited, Essex, UK). Ion-strength adjuster (ISA) for the nitrate ISE was 5 mol L^{-1} ammonium sulfate solution, made with powder (Fluka, Buchs, Switzerland). ISA for the chloride ISE was 5 mol L^{-1} sodium nitrate solution made with powder (Aldrich Chemical Co., Milwaukee, WI, USA). No ISA was used for the Fluoride ISE. Chloride-ISE calibration standards were made by diluting a 1 mol L^{-1} NaCl stock solution, made with the powder (Fisher Scientific Co., Hampton, NH, USA). Nitrate-ISE calibration standards were prepared by sequential dilution of 0.1 mol L^{-1} $NaNO_3$ stock solution (Ionplus, Thermo Orion, Waltham, MA, USA), and this stock solution was also used for the measurement of membrane exchange capacity and selectivity. $NaNO_3$ sample solution (1 mmol L^{-1}) was made similarly. 1 mol L^{-1} of $NaNO_3$ was also prepared with the powder and this nitrate solution was used to exchange chloride ions in ion-exchange membranes with nitrate ions. NaF stock solution at 0.1 mol L^{-1}, purchased from Sigma (Fluka, Buchs, Switzerland), was diluted and used as dialysate, and used in membrane-selectivity measurement as well.

2.2. Measurement of membrane thickness and exchange capacity

Anion-exchange membranes (AEM) Neosepta AFN and ACS (Astom Corp., Tokyo, Japan) were used in this research. Both Neosepta membranes were saturated with chloride ions when received. After the membranes were thoroughly washed with DI water, a rectangular membrane piece ($\simeq 9.7$ cm^2) was stored in 100 mL of 0.1 mol L^{-1} $NaNO_3$ solution in an Erlenmeyer flask for 24 h. Chloride ions in the membrane phase were exchanged with nitrate in the solution phase. During the ion exchange, the flask was tightly sealed from ambient air, and shaken on an orbital mixer (Thermolyne Speed RotoMix M71735, Barnstead International, Dubuque, Iowa, USA). The mixture of nitrate and chloride in the flask was then drained, and stored in a polyethylene bottle. A 100 mL nitrate solution was added one more time, and the ion exchange was repeated. Then the ion exchange was repeated two more times with 50 mL nitrate solution. During this 96 h period, a total of 300 mL of solution was collected for later analysis. The membrane was quickly washed with DI water and blot-dried with filter paper. The thickness was quickly measured with a micrometer at 5 different points (i.e., four corners and center) and the average thickness was calculated.

Assuming that all Cl^- ions are exchanged with NO_3^- ions with one-to-one ratio, the membrane exchange capacity Q was obtained by measuring $\overline{C}_{eq}$ (upper bar denotes membrane phase and the subscript "eq" denotes equilibrium), concentration of chloride in the stored exchange solution with the ISE. Q is given by

$$Q = (\overline{C}_{eq} V_{sol})/V_m = \overline{C}_{eq} V_{sol}/(\delta A_m). \quad (1)$$

where V_{sol} is the solution volume, and V_m the membrane volume ($=\delta \cdot A_m$, where δ is the thickness and A_m is the area.). V_m is measured in a water-saturated condition. Q is the exchange capacity of the wet membrane in Cl^- form and has units of molar concentration [mol L^{-1}]. The membrane piece was dried in an oven at 50 °C for 4 days and the dry weight w_{dry} was measured to calculate Q_{dry} in units of [mol kg^{-1}] with the following expression:

$$Q_{dry} = \overline{C}_{eq}(V_{sol}/w_{dry}). \quad (2)$$

The value of Q_{dry} was used in calculating selectivity coefficient (see the following section for detail). A total of 10 pieces were used to calculate the average of δ and Q.

2.3. Measurement of selectivity coefficient

Selectivity coefficient K determines the equilibrium ionic fraction between the solution and membrane phases. It is defined as

$$K_{NO_3^-}^{F^-} = \frac{\overline{C}_{F^-}/\overline{C}_{NO_3^-}}{C_{F^-}/C_{NO_3^-}} = \frac{x_{NO_3^-}(1-y_{NO_3^-})}{y_{NO_3^-}(1-x_{NO_3^-})}, \quad (3)$$

where the ionic fractions of the solution and the membrane phase are defined respectively as $x_{NO_3^-} = C_{NO_3^-}/(C_{F^-}+C_{NO_3^-})$ and $y_{NO_3^-} = \overline{C}_{NO_3^-}/(\overline{C}_{F^-}+\overline{C}_{NO_3^-})$. Measurement of $x_{NO_3^-}$ is straightforward, but $y_{NO_3^-}$ can only be measured indirectly from the concentration change in solution in equilibrium with membrane, that is the difference between initial (before equilibrium) and final concentrations (after equilibrium) in solution phase [32] [see Supplementary Data (SD) Section S.1.1 for detail].

Ten 2.5 cm × 3 cm membrane pieces were thoroughly washed with DI water. All Cl^- ions were exchanged with nitrate in 100 mL of 1 mol L^{-1} $NaNO_3$ solution. Ten 250 mL equilibrating solutions with different ratios were prepared (i.e., NaF:$NaNO_3$=1:0, 0.04:0.96, 0.1:0.9, 0.2:0.8, 0.3:0.7, 0.4:0.6, 0.6:0.4, 0.7:0.3, 0.8:0.2, and 0.9:0.1, the total concentration of 0.01 mol L^{-1}). The membrane was stored in each equilibration solution for 3 days. The flask was sealed and agitated during equilibration. The initial and final concentrations of NO_3^- and F^- in each equilibrating solution were measured. The exchange capacity Q is required to calculate K (see Section S.1.1 in SD for detail). Instead of Q for wet membrane, Q_{dry} value was obtained by measuring dry weight of membrane w_{dry} and using Eq. (2) because of the difficulty in accurately measuring wet volume V_m of a membrane piece. After equilibration, the membrane pieces were dried for 4 days in an oven at 50 °C, and weighed to determine w_{dry} (see Section S.1.2 in SD for detail).

K was found to be a monotonically increasing function of $x_{NO_3^-}$. An exponential function

$$K(x) = b_0 + a_0 e^{a_1 x}, \quad (4)$$

represents the behavior of K satisfactorily [33,34]. Sigmaplot software (Systat, San Jose, USA) was used for curve fitting.

2.4. Fabrication of continuous stirred-tank Donnan dialyzers (CSDD)

Two continuous stirred-tank Donnan dialyzers (CSDD) were designed and fabricated to analyze the irreproducibility. The dialyzer was made of Plexiglas using conventional machining techniques. The first CSDD has cubic dialystate/sample containers. The container dimension was 2.54 cm × 2.54 cm × 2.03 cm (=13 mL) and a cross-type magnetic stir bar was inside the container for agitation. The second CSDD has a unique long and low-profile container. The length of the container was 10.35 cm and the cross sectional area is 3.04 cm wide × 0.32 cm tall (i.e., volume=10 mL). Long (2.84 cm) and slender (0.28 cm diameter) magnetic stir bars were used in the low-profile containers. All stir bars are from Big Science Inc. (Huntersville, NV, USA). AEMs were sandwiched between the two containers. The containers were leak-free as tightly joined by screws and nuts. A custom-made stirrer was used to spin the magnetic stir bars inside our CSDDs. The stirrer has a strong permanent magnet, rotated by a dc motor (MicroMo Electronics, Clearwater, FL, USA). The motor is controlled by a dc power supply (E3630A, Agilent, Santa Clara, CA, USA). The rotation speed was set to be 1300 RPM because mass transport was not improved at faster speeds.

2.5. Fabrication of parallel-plate Donnan-dialytic membrane-separation module (PDMM) with recirculation tubes

The PDMM consists of the two identical Plexiglas parallel plates facing each other and an AEM between them as shown in Fig. 1a. Each plate has 400 μm-deep, 6 mm-wide (widest point), and 12.5 mm-long (longest point) microfluidic channel, machined by milling. The shape of the microchannel is tapered at both ends for a smooth dimensional transition. The channel has a support pillar (1 mm wide and 8.8 mm long) in the center to prevent membrane rupture (detail follows in Section 2.6). The effective width of the microfluidic channel is 5 mm considering the width of the pillar. The exposed area of the membrane is 50 mm^2 (i.e., the dark area on the AEM in Fig. 1a). The AEM is placed between the two parallel plates and tightly secured with screws and nuts. A small-bore tube is connected to a parallel plate to form a closed loop. Barbed fluidic connectors are attached to the inlet and outlet (not shown in the figure), to which recirculation tubes are securely connected. The tube is 4.54 m long and 1/16 inch-diameter FEP-lined Tygon tubing (Saint-Gobain, Akron, OH, USA). No leakage was observed without a gasket.

2.6. Fluidic circuit for PDMM experiment

Dialysis process of the PDMM is illustrated in Fig. 1b. One end of each tube is connected to a PDMM outlet and the other end of the tube is connected to an input of a peristaltic pump. The peristaltic pump (Masterflex console driver, 77521-50, and Easy load II pump head, 77200-60, Cole-Parmer, Vernon Hills, IL, USA) was used to force solution through the tube. The peristaltic pump is connected to a custom-made valve manifold in which two 3-way inert microsolenoid valves (LHYA1215010H, The Lee Company, Westbrook, CT, USA) are linked in series. The valve manifold steers solutions into or out of the recirculation loop with the following procedure: (1) During the “load” mode, the dialysate side of fluidic circuit is connected to a fresh dialysate solution and a downstream detector. Simultaneously the sample side is connected to a fresh sample and waste. The fresh dialysate and sample solutions are introduced to each recirculation loop. At the same time, processed sample solution is flushed away to waste and analyte-containing dialysate solution is delivered to the downstream detector and (2) during the “dialysis” mode, the fluidic circuit is isolated from the outside to form a closed fluidic loop. Solution circulates inside each loop through the PDMM, tube coil, peristaltic pump, and then valve manifold. After the dialysis is completed, the valve manifold is set to “load” mode again and dialysis steps (1) and (2) are repeated. The valves and peristaltic pump were controlled by PC using LABVIEW software (National

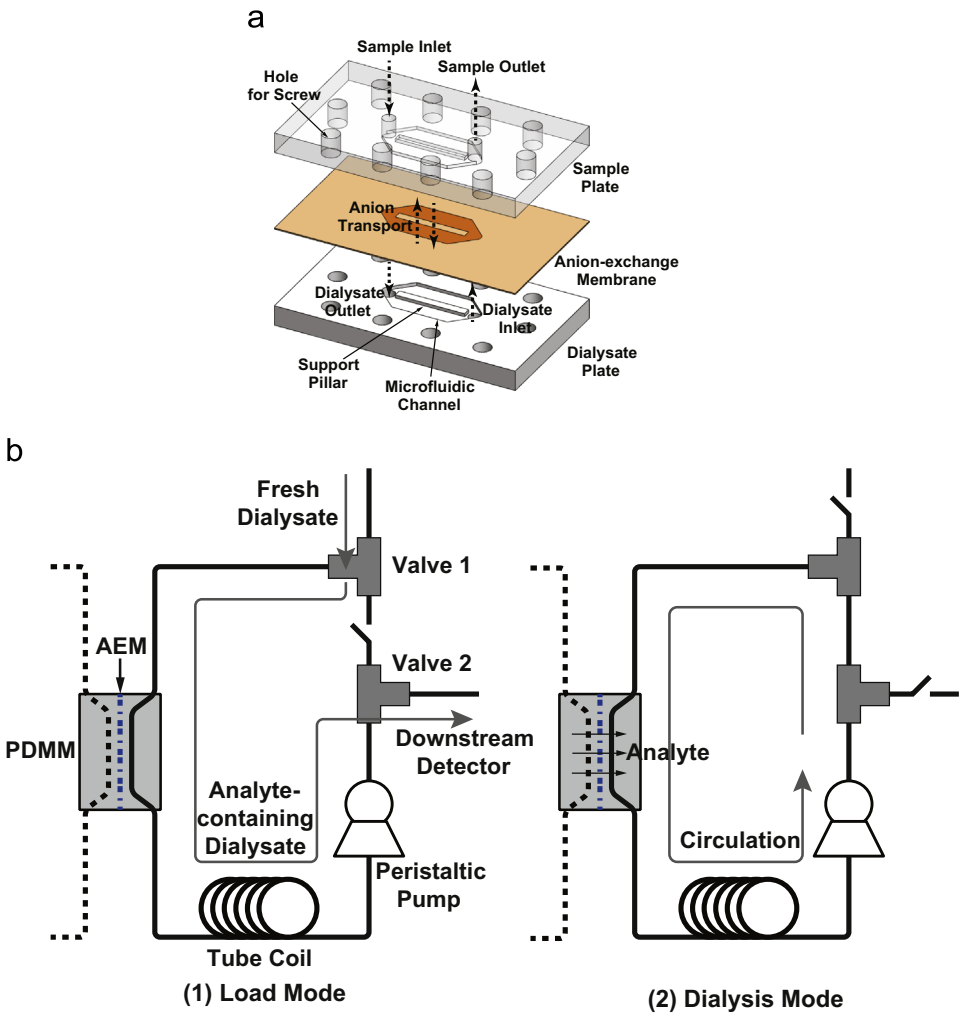

Fig. 1. The parallel-plate Donnan-dialytic membrane-separation module (PDMM) with recirculation loop. (a) Exploded view of the parallel-plate dialyzer unit and (b) two operational stages of the PDMM (the dialysate side is shown in solid line and the sample side is expressed in dotted line): (1) the sample and dialysate solutions are introduced into the recirculation loop, and at the same time the previously processed solutions are flushed away; (2) newly injected solutions are recirculated in the closed loop for Donnan dialysis.

Instruments, Austin, TX, USA) and a data-acquisition (DAQ) board (NI-6024E, National Instruments). A custom-made relay circuit (Hamlin HE721A051U, Digikey, Thief River Falls, MN, USA) and the power supply (E3630A, Agilent) were used to provide enough current to the valve manifold. For fluidic couplings, Luer-Loks made of Kynar were used. No leakage was observed in the fluidic circuit up to flow rate of 60 mL min^{-1}.

After the transition from the load mode to the dialysis mode, a dead volume of the solenoid valves coagulated into an air plug. The air plug trailed the solution in the recirculation loop. Cycles of the two solutions were not synchronized, and the two asynchronized air plugs resulted in differential pressure inside the PDMM unit. Therefore, the membrane collapsed to one side and then to the other side, which caused membrane fatigue and finally rupture. The support pillar in the microfluidic channel effectively prevented membrane rupture.

2.7. Numerical simulation

Irreproducibility in Donnan dialysis was analyzed using a numerical simulation code written in MATLAB (Mathworks, Natick, MA, USA). Simulation parameters including membrane property and dialyzer dimension were measured in house.

2.8. Dialysis experiment

The dialysis experiments were performed (1) to confirm the presence of the theoretically predicted irreproducibility, and (2) to characterize performance metrics of the novel PDMM. After the ion exchange with nitrate was completed, AEM pieces were stored in agitated DI water for 24 h to remove residual nitrate and sodium ions. The cleaned membrane pieces were used in dialysis experiments. A model bi-ionic system for the experiment was 1 mmol L^{-1} $NaNO_3$ |AEM| 10 mmol L^{-1} NaF. Lacking a sensor installable inside the PDMM, the time-dependent dialysis process was monitored *ex situ*. The dialysis process was repeated for decreasing durations (e.g., 75, 47, 36, 24, 22, 16, 12, 6, 3, 2, 1.5, 0.75, 0.5, 0.25 h). Both dialysate and sample solutions were collected after each dialysis, and then nitrate concentration was measured with the ISE. Four different flow rates (0.163, 0.267, 0.378, and 0.454 ms^{-1}) were used to study the effect of the flow rate on the throughput. The temperature was regulated at 22.4 ± 1 °C.

For investigation of hydrodynamic condition in the recirculation tube, a Kenics in-line static mixer (GracoOhio, North Canton, Ohio, USA) was installed between the PDMM outlet and the tube coil. The 1/8 inch-diameter static mixer was 3 inches long and had 24 mixing elements.

3. Results

3.1. Membrane-property characterization

The selectivity coefficients K for both the Neosepta membranes in the NaF+$NaNO_3$ solution were obtained. Nonlinear regression ($R^2 = 0.996$) yielded the selectivity coefficient of the ACS membrane (See Fig. S.1 in SD):

$$K = 0.0049 + 0.0106e^{(2.7010x_{NO_3^-})}. \quad (5)$$

The role of selectivity coefficient is to determine ionic fraction of membrane phase $y_{NO_3^-}$ as a function of solution-phase ionic fraction $x_{NO_3^-}$. We plot the measured $y_{NO_3^-}$ as a function of $x_{NO_3^-}$ as in Fig. 2 (solid circle). The figure also depicts the estimated $y_{NO_3^-}$ (inverted triangle) and an extrapolated $x-y$ curve (solid line). We noted from Fig. 2 that the measured and estimated $y_{NO_3^-}$ using Eq. (5) agreed pretty well. The extrapolated curve follows the trend of $y_{NO_3^-}$ nicely for varying $x_{NO_3^-}$ value between 0 and 1. From this figure, the selectivity coefficient does represent equilibrium between membrane and solution phases well.

The selectivity coefficient of an AFN membrane was calculated in the same manner (Fig. S.2a in SD). Curve fitting resulted in ($R^2 = 0.977$):

$$K = 0.0065 + 0.0093e^{(3.3343x_{NO_3^-})}. \quad (6)$$

For the AFN membrane, the estimated membrane-phase ionic fraction agreed well with the measured value (Fig. S.2b in SD). Both membranes show greater affinity toward nitrate than fluoride even though the two ions have the same valance. The preferential affinity is well documented in the literature [35] and may be attributed to difference in solvated size and hydrophobicity of ions. Nitrate is smaller and more hydrophobic than fluoride [36]. In order to reduce membrane swelling, an AEM tends to prefer smaller ions [35]. Both ACS and AFN membranes are prepared by copolymerization of styrene and divinylbenzene [37,38]. Hydrophobic polystyrene resins may prefer more hydrophobic nitrate ions [39].

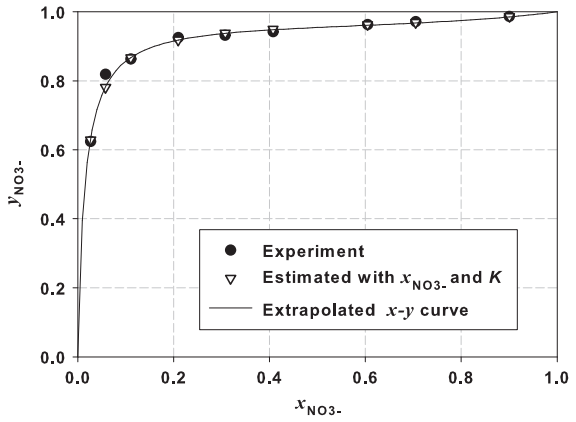

Fig. 2. Ionic fraction of NO_3^- in the membrane phase $y_{NO_3^-}$ as a function of the ionic fraction in the solution phase $x_{NO_3^-}$.

Table 1
Properties of the ACS and AFN membranes characterized in this work.

Membrane property	Neosepta ACS	Neosepta AFN
Thickness [mm]	0.123	0.153
Exchange capacity ([M], wet, Cl^- form)	1.91	4.36
Exchange capacity ([mol kg^{-1}], dry, Cl^- form)	1.89	5.16
Selectivity Coefficient ($K^{F^-}_{NO_3^-}$)	$0.0049+0.0106e^{2.7010x}$	$0.0065+0.0093e^{3.3343x}$

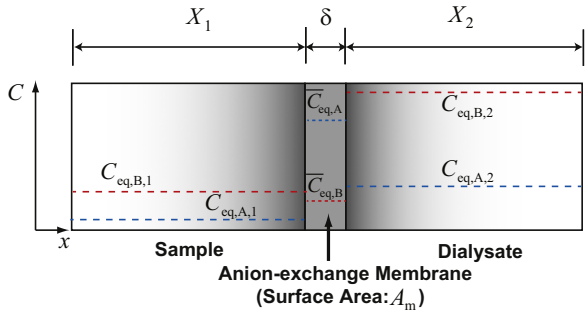

Fig. 3. Schematic diagram for Donnan equilibrium of a bi-ionic system in a CSDD.

The $x-y$ curves for the both membranes are monotonically increasing functions, adequate for the numerical analysis conducted in this study because a $y_{NO_3^-}$ value is uniquely defined for a $x_{NO_3^-}$. The measured membrane properties are summarized in Table 1.

3.2. Analysis of Donnan-dialyzer irreproducibility

3.2.1. Derivation of equation for the equilibrium sample/dialysate concentration of a CSDD

Let us consider a simple bi-ionic system in a CSDD in equilibrium as shown in Fig. 3. The CSDD has two containers of the same width and height, facing each other with an AEM between them. The width and height of the AEM are also same as those of the containers. Here we assume that ions move only in x direction. The length of the sample container, the dialysate container, and the membrane are X_1, X_2, and δ, respectively (subscript 1 denotes the sample and 2 the dialysate side respectively). Equilibrium concentrations in membrane phase $\overline{C}_{eq}$ and solution phase C_{eq} of species A and B are represented as dashed lines (note that membrane-phase concentrations are orders-of-magnitude larger than solution-phase concentrations). Perfect agitation and thus uniform concentration profiles in both containers are assumed.

Equilibrium concentration of species A in membrane phase $\overline{C}_{eq,A}$ can be obtained by solving a polynomial equation derived using Nernst–Planck equation and Donnan equilibrium equation (See Section S.1.3 in SD for detail):

$$(K-1)V_m\overline{C}^2_{eq,A} + [M_A(1-K)+V_mQ+K(V_1C_{T,1}+V_2C_{T,2})]\overline{C}_{eq,A} - M_AQ = 0, \quad (7)$$

where M_A is the total mass of species A, C_T is the total concentration of counterions in solution phase, and V is the volume. This equation does not have analytical solutions because the selectivity coefficient K is an exponential function. Thus the equation must be solved numerically. Equilibrium concentration of species A in the dialysate solution, that is the dialyzer output, is given by

$$C_{eq,A,2} = (M_A - V_m\overline{C}_{eq,A})/\left(V_2 + V_1\frac{C_{T,1}}{C_{T,2}}\right). \quad (8)$$

The rest of the equilibrium concentrations in the membrane and the solution phases can be calculated using Donnan-exclusion and mass-conservation conditions [See Eqs. (S.13), (S.14), and (S.28) in SD].

For the case where the length and thus the volume of the two containers are identical [$X_1 = X_2$, $V_1 = V_2 (= V)$], Eq. (8) can be written as

$$C_{eq,A,2} = \frac{(M_A - V_m\overline{C}_{eq,A})/V}{1+C_{T,1}/C_{T,2}} = \frac{C_{A,T}+1/R_V(\overline{C}_A - \overline{C}_{eq,A})}{1+C_{T,1}/C_{T,2}}, \quad (9)$$

where $R_V(=V/V_m=X/\delta)$ is defined as solution-to-membrane volume ratio. If one repeats dialysis process without changing the AEM inside the dialyzer, $\overline{C}_A$ value is continuously updated throughout multiple dialysis steps. The final (i.e., equilibrium) concentration value of the prior dialysis step $(k-1)$ is carried over to the initial concentration value of the present dialysis step (k) $[\overline{C}_A(k)=\overline{C}_{eq,A}(k-1)]$. Therefore, we have the dialyzer output at step (k):

$$C_{eq,A,2}(k)=\frac{C_{A,T}(k)+1/R_V[\overline{C}_{eq,A}(k-1)-\overline{C}_{eq,A}(k)]}{1+C_{T,1}(k)/C_{T,2}(k)}. \quad (10)$$

In general the solution to Eq. (7) at each step is different $[\overline{C}_{eq,A}(k)\neq\overline{C}_{eq,A}(k-1)]$ even if all the other solution-phase parameters are equal because $M_A(k)$ varies as a function of $\overline{C}_{eq,A}(k-1)$ [See Eq. (S.11)]. Eq. (10) shows that the dialyzer output $C_{eq,A,2}(k)$ varies if we repeat the dialysis process even without changing solution-phase dialysis condition.

If one increases the solution-to-membrane volume ratio infinitely large $(R_V\to\infty)$, Eq. (10) simply becomes

$$C_{eq,A,2}(k)=\frac{C_{A,T}(k)}{1+C_{T,1}(k)/C_{T,2}(k)}. \quad (11)$$

It is noted that $C_{eq,A,2}(k)$ is now determined by only solution-phase concentrations. Eq. (11) is indeed identical to the expression for the dialyzer output in ideal Donnan equilibrium where the counterion storage effect of the AEM is completely disregarded (see S.1.4 in SD for detail). $C_{eq,A,2}(k)$ remains equal unlike Eq. (10) as long as the equal initial solution-phase concentrations are used for repeated dialysis. It is interesting to note that the dialyzer output becomes close to the ideal value $(C_{eq,A,2}(k)\to C_{eq,A,2}|_{ideal})$ and increasingly reproducible if R_V increases. Therefore, R_V is the key parameter that determines irreproducibility of a CSDD and gauges how close a CSDD to the ideal Donnan dialyzer.

Let us define "dialyzer state" as equilibrium solution- and membrane-phase concentrations for discussion in the following sections. The prior dialyzer state at $(k-1)$ step affects the state at (k) step if R_V value is finite. The dialysis is irreproducible in this condition. On the other hand, the dialyzer state (k) is independent of the prior state $(k-1)$ and the dialysis is completely reproducible if R_V is infinite.

3.2.2. Numerical analysis of the Donnan-dialyzer irreproducibility

The impact of dialysis conditions to the dialyzer irreproducibility is studied using numerical analysis. The Donnan-equilibrium concentrations [from Eqs. (7) to (8)] was numerically solved using a MATLAB code. The model bi-ionic system for a CSDD was x mmol L^{-1} $NaNO_3$ |ACS| 10 mmol L^{-1} NaF. The lengths of the both containers were identical. The cross-sectional areas of the containers and the membrane were also equal (i.e., A_m). The length of containers was varied to study the effect of R_V on the irreproducibility. We assumed that initially species A (i.e., analyte) existed only in the sample solution and species B (i.e., concentrated driving ions) existed only in the dialysate solution. The dialysate concentration was fixed at 10 mmol L^{-1} (or 0.01 kmol m^{-3}) all the time. Three types of numerical simulations were conducted by changing initial analyte concentration $C_{A,1}$ (i.e., the dialyzer input) during multiple dialysis steps: $C_{A,1}$ was (1) constant, (2) varied randomly, and (3) varied incrementally. Each condition was examined for a specific operation scenario of a CSDD-equipped analytical system: (1) the reproducibility of the analytical system is characterized; (2) random samples are analyzed; and (3) the analytical system is calibrated, respectively. The case (1) is also useful in understanding the concept of dialyzer irreproducibility and in quantitatively comparing irreproducibility of the CSDDs with different geometry and membrane properties (see Section 3.2.3 and Table 2). Throughout the numerical simulation, R_V was varied to examine its impact on the irreproducibility. The other parameters were fixed (see the simulation parameters listed in Table S.1 in SD).

3.2.2.1. Case 1: Dialysis repeated with a constant initial sample concentration. The initial sample concentration was fixed to $C_{A,1}=1$ mmol L^{-1} in the first case of numerical analysis. For a total of 4 batches of simulations, R_V values 10, 100, 1000 and 10,000 were employed. For each batch, the dialysis was repeated 20 times. Fig. 4a shows that equilibrium concentration of species A in dialysate $C_{eq,A,2}$ decreases asymptotically and converges to a constant value as the dialysis step increases. The converging value was $C_{eq,A,2}|_{ideal}$, the dialysate concentration of species A in ideal Donnan equilibrium (i.e., $R_V\to\infty$). Using Eq. (11), $C_{eq,A,2}|_{ideal}$ was calculated to be 0.9091 mmol L^{-1}. For all the R_V values $C_{eq,A,2}$ eventually converged to 0.9091 mmol L^{-1}, but for the smaller R_V values the more dialysis steps are required for convergence. For larger R_V values, $C_{eq,A,2}$ converges more rapidly because the dialysis condition is more ideal.

Fig. 4b shows that perfectly reproducible dialyzer responses when the membrane is put back to the original state after each dialysis step. In this condition, $\overline{C}_{eq,A}(k-1)$ is constant, and therefore $M_A(k)$ is constant as well. The solution to Eq. (7), $\overline{C}_{eq,A}(k)$, is also constant. Consequently, $\overline{C}_{eq,A}(k-1)-\overline{C}_{eq,A}(k)$ is constant, and $C_{eq,A,2}(k)$ of Eq. (10) becomes constant throughout multiple dialysis steps. $C_{eq,A,2}(k)$ depends on only the R_V value and the initial solution-phase concentrations at step (k), not the prior dialyzer state at step $(k-1)$. From the figure we note that the bigger the R_V, $C_{eq,A,2}(k)$ is the closer to $C_{eq,A,2}|_{ideal}$. However, putting the membrane back to the original state by saturating with nitrate is impractical because it would be time consuming (e.g., more than a day).

Table 2
Performance comparison the three types of Donnan dialyzers.

Dialysis condition and dialyzer performance	CSDD with cubic containers		CSDD with low-profile containers		PDMM with recirculation tubes	
	ACS	AFN	ACS	AFN	ACS	AFN
Solution volume [mL]	13	13	10	10	10	10
Solution-to-membrane volume ratio (R_V)	207	166	842	676	1577	1268
Irreproducibility[a] [step]	4	8	2	3	2	2
Equilibrium time [h]	2	0.5	75	–	12[b]	1[c]

[a] Dialysis step required to reach within 10% error of $C_{eq,A,2}|_{ideal}$ value.
[b] Flow rate is 0.163 ms^{-1}.
[c] Flow rate is 0.454 ms^{-1}.

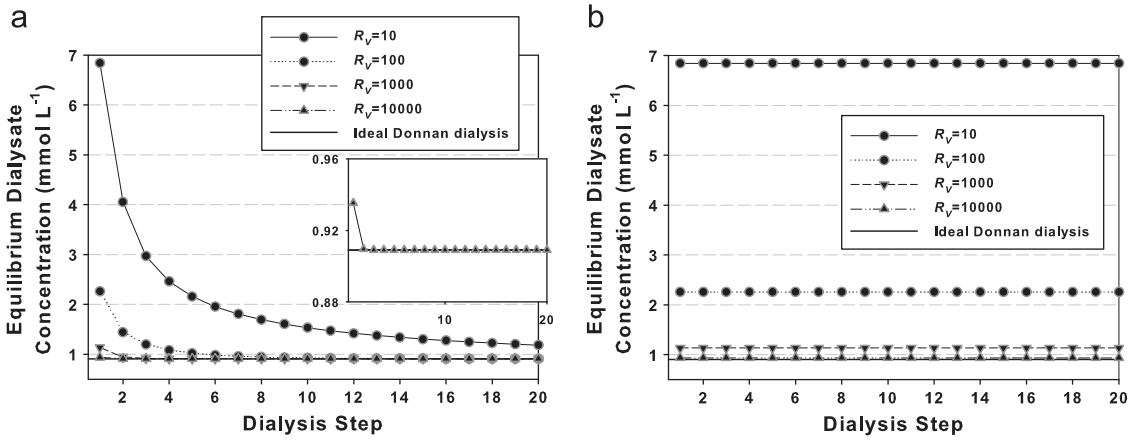

Fig. 4. Numerical analysis results for CSDD responses (Case 1). $C_{eq,A,2}$ values are shown when dialysis is repeated with a constant $C_{A,1}$. (a) The prior dialyzer state is considered. The inset figure shows magnified graph for $R_V = 10,000$ and (b) the prior dialyzer state is disregarded.

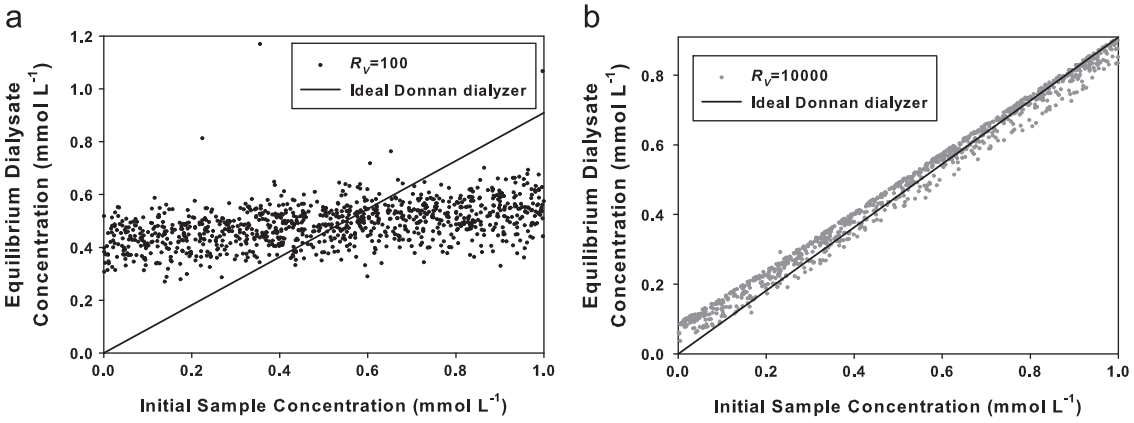

Fig. 5. Numerical simulation results for input–output characteristics of a CSDD (Case 2). $C_{eq,A,2}$ values are shown when dialysis is repeated with the sample concentration changed randomly and (a) $R_V = 100$ and (b) $R_V = 10,000$. The solid line denotes the ideal input–output characteristic.

3.2.2.2. Case 2: Dialysis repeated with random initial sample concentration. To analyze irreproducibility in an analytical-system standpoint, input–output characteristics of the dialyzer are studied (Fig. 5). The *x*-axis denotes $C_{A,1}$, that is the input to the dialyzer. The *y*-axis refers to $C_{eq,A,2}$, that is the output of the dialyzer. The input–output relation of an ideal dialyzer for an analytical system should be linear over a wide concentration range.

1000 of $C_{A,1}$ values were randomly selected within the range of [0, 1] mmol L^{-1}. Fig. 5a shows a simulation result for the case where the prior dialyzer state is considered (R_V=100). The output of the dialyzer was randomly spread within the range [0.299, 2.15] mmol L^{-1}. No correlation between input and output was noted. The ideal input–output characteristic (solid line, $R_V \to \infty$) is also depicted as a reference. When R_V was the largest (10,000), the CSDD response was distributed around the reference curve with a certain extent of randomness as seen in Fig. 5b. However, the correlation between the input and the output was clearly observed ($R^2 = 0.99$). Irreproducibility of the dialyzer apparently decreased, compared with Fig. 5a. The wide distribution of the dialyzer output would result in reduced precision of the entire analytical system. LOD (limit of detection) could also be increased as the *y*-intercept was not 0 anymore, and there existed a random distribution around the intercept (i.e., 0.055). As with Case 1, the dialyzer was 100% reproducible when the prior dialysis state was not considered; the random distribution of the dialyzer output was not observed anymore (see Fig. S.3 in SD).

3.2.2.3. Case 3: Dialysis repeated with increasing initial sample concentration. In the third analysis, $C_{A,1}$ is increased from 0.001 to 1 mmol L^{-1} in each batch of simulations (i.e., $C_{A,1} = 0.001 \cdot 2^n$ mmol L^{-1}, $n = 1, 2, \ldots, 10$) to study linearity of the dialyzer. The same four R_V values were also used for the four batches of simulations. Fig. 6a shows the simulation results. The solid line indicates input–output relation of the ideal dialyzer. The slope of the solid line is 0.9091. A significant nonlinearity was observed when R_V was small. The small concentration of species *A* (i.e., <1 mmol L^{-1}), originating from the sample solution, was "swamped" by the species *A* of the membrane phase in high concentration (i.e., typically >1 mol L^{-1}). The input-to-output ratio of species *A* was substantially larger than 1 for small R_V values because a large amount of species percolated out of the membrane, and thus significantly increased $C_{eq,A,2}$. The linearity was improved when R_V increased. For R_V=1000 and = 10,000, the input–output relation changed from convex-downward curves to straight lines as the dialysis step repeats. When $C_{A,1}$ was low, species *A* from the sample solution was still overshadowed even at these high R_V values. However, a larger and larger portion of the species *A* was transferred from the membrane as the dialysis step repeats. As $C_{A,1}$ increased, the contribution of $C_{A,1}$ to the dialyzer output $C_{eq,A,2}$ also grew. Eventually, $C_{A,1}$ became the dominant source of the dialyzer output, and the input–output relation became linear. Such transitions happened earlier for large R_V values. When R_V was 10,000, the response curve was linear

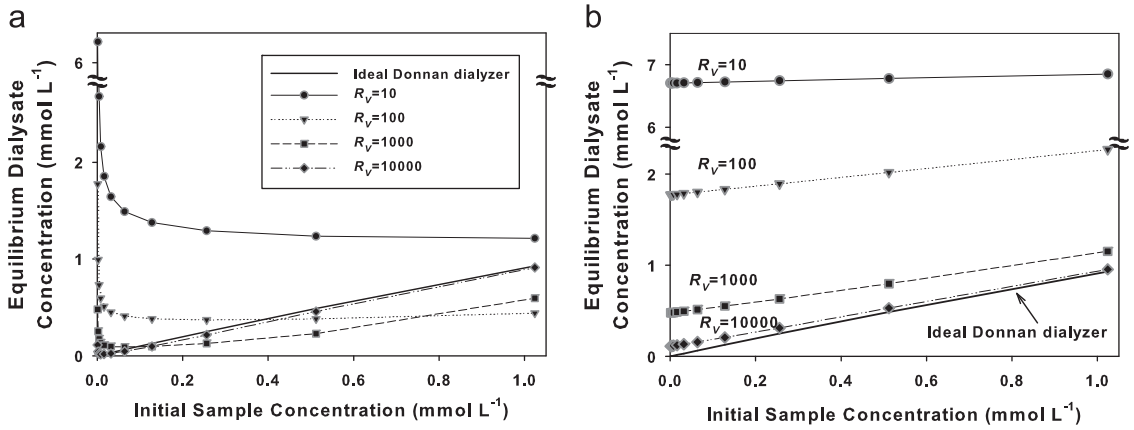

Fig. 6. Numerical simulation results for input–output relations of a CSDD (Case 3). $C_{eq,A,2}$ (i.e., output) values are shown when dialysis is repeated with the sample concentration (i.e., input) changed incrementally and (a) the prior dialysis state is considered and (b) disregarded. The solid line denotes the ideal input–output relation.

($R^2 = 0.999$) for $C_{A,1}$ values from 0.008 to 1 mmol L^{-1} (the 3 lowest concentrations are not included). However, a nonlinearity was still observed in a low-concentration range (see Fig. S.4 in SD). As a result, nonlinearity of low $C_{A,1}$ values would increase LOD of the entire analytical system.

When the prior dialysis state was not considered, the linearity was 1 ($R^2 = 1$) regardless of the solution volume as seen in Fig. 6b. However, the slope was always smaller than 0.9091. The slope became closer to 0.9091 (i.e., the ideal Donnan equilibrium) for the larger R_V values. A y-intercept was much larger than 0 for small R_V values (e.g., R_V=10 and 100). The increased y intercept could lead to an increase in the LOD of the entire analytical system (i.e., background signal increase). The slope affects the sensitivity of the dialyzer and thus the sensitivity of the analytical system. Therefore, large R_V is preferable for small LOD and large sensitivity.

3.2.3. Experimental verification of the donnan-dialyzer irreproducibility

Throughout the three cases of numerical simulations, we noted that large R_V was preferred for sensitivity, precision and LOD of the entire analytical system. Dialysis experiment was performed to confirm the irreproducibility predicted by the numerical analysis. A CSDD with cubic containers and a CSDD with long, low-profile containers were employed for the experiment. Limitations of a CSDD as a sample preparation module for an analytical system are given to motivate our PDMM.

3.2.3.1. Dialysis experiment using a CSDD with cubic containers. Firstly, time required for equilibrium was measured to determine throughput of the sample-preparation module. The concentration change of the sample and dialysate in the CSDDs was monitored over time. Fresh solutions were supplied to the containers and the dialysis was performed for a period of time. The dialysis period was changed decrementally, and the sample/dialysate concentrations were measured using ISEs after each period. The equilibrium is reached in roughly 2 h for an ACS membrane. The CSDD with an AFN membrane shows a reasonable speed (i.e., 30 min). The transport through the ACS membrane is much slower because of highly crosslinked polymer layer grafted on the membrane surface for monovalent selectivity [40].

Secondly, irreproducibility of the CSDD was characterized. Dialysis is repeated with a constant initial condition (i.e., 1 mmol L^{-1} $NaNO_3$ |AEM| 10 mmol L^{-1} NaF). The prior dialyzer state is considered without changing the AEM inside the CSDD. We clearly observed a significant variation in the dialyzer output throughout multiple dialysis steps for the both membranes as in Fig. 7. For comparison, numerical analysis results are also shown in the figure. As the exchange capacity of the AFN membrane was bigger than that of the ACS membrane (i.e., Q=4.36 vs. 1.91 mol L^{-1}), the dialyzer output in early dialysis steps was more deviated from $C_{eq,A,2}|_{ideal}$ (=0.9091 mmol L^{-1}), because a larger amount of nitrate stored in the AFN membrane diffused into dialysate (Fig. 7b). It took 9 steps to reach within 10% error of the $C_{eq,A,2}|_{ideal}$ value for the ACS membrane, and 15 steps for the AFN membrane. Although R_V is similar for both membranes (i.e., 207 for the ACS membrane and 166 for the AFN membrane), the dialyzer output for the ACS membrane converges to the $C_{eq,A,2}|_{ideal}$ value faster because of smaller initial deviation than that for the AFN membrane.

The reason for a serious irreproducibility of the dialyzer output is small solution-to-membrane mass ratio of species A. Total mass of ions per unit area is 123 μm · 1.91 mol L^{-1} = 0.235 mol m^{-2} for the ACS membrane and 153 μm · 4.36 mol L^{-1} = 0.667 mol m^{-2} for the AFN membrane. The total mass of the membrane-phase counterions is similar or more than that in the sample or dialysate solution (i.e., 25.4 mm · 1 mmol L^{-1} = 0.0254 mol m^{-2} for the sample and 25.4 mm · 10 mmol L^{-1} = 0.254 mol m^{-2} for the dialysate solution). Consequently, the membrane acts as a counterion storage, and the stored counterions affects the dialyzer output in subsequent dialysis steps, showing dependence on the prior dialyzer state. This irreproducibility renders the CSDD practically unusable.

The experimental results were compared with the numerical simulations. It took 4 steps to reach within 10% error of the $C_{eq,A,2}|_{ideal}$ value for the ACS membrane and 8 steps for the AFN membrane. Fig. 7 indicates the numerical model agrees reasonably well with the dialysis experiment, and thus the measured membrane parameters are generally valid. Discrepancy between the simulation and experimental results may be attributed to a low accuracy of ISEs or dependence of selectivity coefficient K on ionic strength [41] (we assumed otherwise, see Section 2.3).

3.2.3.2. Dialysis experiment using a CSDD with long, low-profile container. Samples are usually in much lower concentration than membrane phase in our experimental condition (~0.01 vs. ~1 mol L^{-1}). Therefore, R_V should be sufficiently large. If we scale up the cubic CSDD container [e.g., 10 cm × 10 cm × 10 cm(=1 L)], irreproducibility issue will be alleviated owing to an increase in the quantity of counterions in the solution phase relative to that in the membrane phase. However, it is impractical for microanalytical systems to deal with such large solution volume. One way to increase R_V while keeping the overall volume small is to use a low-profile dialyzer of

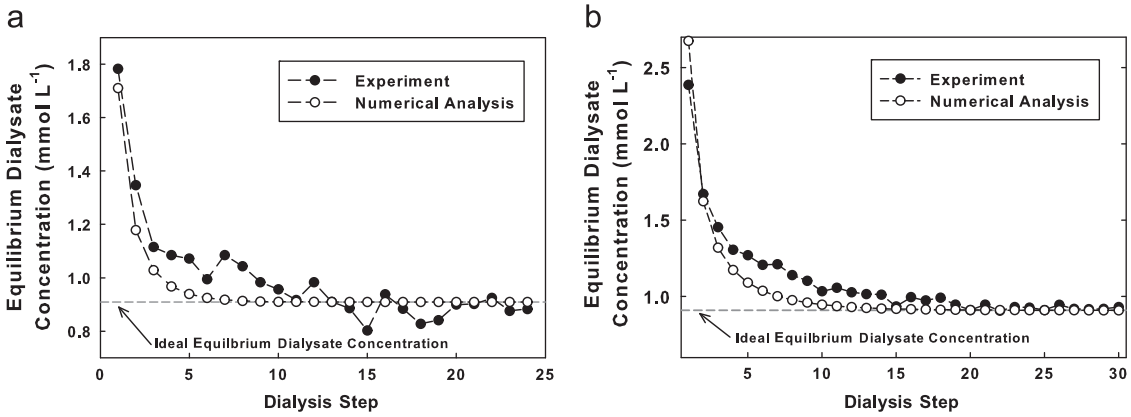

Fig. 7. $C_{eq,A,2}$ values of the CSDD having cubic containers with (a) the ACS membrane and (b) the AFN membrane. Donnan-dialysis was repeated with a constant initial condition: $C_{A,1}=1$ mmol L^{-1}, $C_{A,2}=0$ mmol L^{-1}, $C_{B,1}=0$ mmol L^{-1}, and $C_{B,2}=10$ mmol L^{-1}.

substantially decreased height (0.32 cm) but increased length (10.35 cm). The width was as large as that of the cubic container (i.e., 3.04 cm). It must be emphasized that the solution-to-membrane length ratio is the only dimensional variable determining R_V because the cross sectional area of the membrane and the containers are identical. R_V was 842 for the ACS membrane and 676 for the AFN membrane, much larger compared to the CSDD with cubic containers (i.e., 207 for the ACS membrane and 166 for the AFN membrane, respectively)

However, the equilibrium time for the CSDD with a low-profile container was much slower; it took about 75 h for the dialyzer to reach equilibrium. Effective mixing in such a long and low-profile container was very difficult even with vigorous rotation of magnetic stir bars. The low-profile design was not usable in practice, regardless of theoretical reduction in dialyzer irreproducibility.

3.3. Design and test of a parallel-plate Donnan-dialytic membrane-separation module (PDMM) with recirculation tube

3.3.1. Motivation for the PDMM with recirculation tubes

Numerical analysis and experimental verification clearly show that simple scaling down of a CSDD would not render it suitable for microanalytical systems owing to the irreproducible and nonlinear input–output relationship. We note that the irreproducibility stems from the fact that the dialyzer output strongly depends on the prior dialyzer state. Such dependency becomes significant especially when the total mass of the counterions in the solution phase is in the same order of magnitude as the counterion mass in the membrane phase or less. This phenomenon was hardly an issue in the literature because a large sample volume (50–1000 mL) and/or concentration (50–500 mmol L^{-1}) were commonly used. However, environmental and clinical analyses usually deal with diluted samples of a small volume. Therefore, only way to address this issue is to maximize R_V. At the same time, we want effective mixing to improve dialysis throughput to address the limitation of the CSDD with low-profile containers. Here we propose a novel PDMM with recirculation tubes in order to solve these conflicting analytical problems.

3.3.2. The PDMM with recirculation tubes

A novel way to improve reproducibility is connecting long, small-bore tubes to a microfluidic parallel-plate dialyzer in a closed loop and using a small membrane piece. The tubes themselves serve as the sample and dialysate containers. In this way, solution volumes are still kept low (~10 mL), but a high R_V value can be achieved. Also, effective "agitation" is achieved by forcing the solutions through the tubes.

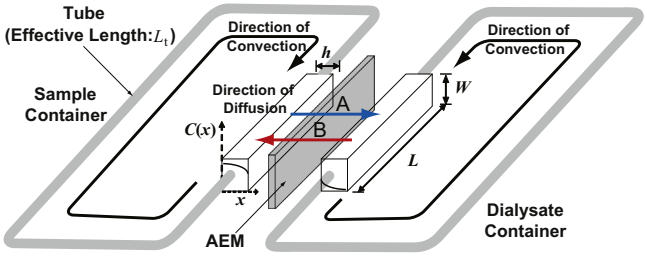

Fig. 8. Schematic diagram of the parallel-plate dialyzer with recirculation tubes.

Fig. 8 portrays a schematic diagram of the PDMM. The dialyzer consists of two "thin" microchannels (i.e., width W, length L, and height h) and an AEM between the two channels. Ionic transport is assume to be only in x direction. Therefore, concentration profile is uniform throughout the width W and the length L. Both ends of a tube are connected to the inlet and outlet of the microchannel. The cross-sectional area of the tube A is selected to be same as that of the microchannels (i.e., $A=W\cdot h$). The length of the tube is 4.54 m. However, the effective length of the tube L_t is 4.85 m including other components in the fluidic circuit: the parallel-plate channel, fluidic couplings, peristaltic-pump tubing, and the inner volume of the solenoid-valve manifold.

3.3.2.1. Working principle of the PDMM. Theoretical analysis on dialysis process may provide useful insights in designing a high-throughput, reproducible PDMM. Early research includes study of mass-transport phenomena in a flow-through parallel-plate dialyzer for neutral species [42,43], a flow-through dialyzer for ionic species [44], and a parallel-plate dialyzer with sample-loop recycle for neutral species [45]. Rigorous numerical analysis of transient mass transport in the PDMM is very challenging [46] and beyond the scope of this study. We will present it in our next communication. Here we lay out a conceptual analysis of the working principle, which is still beneficial, providing a qualitative design guideline.

Working principle behind the proposed PDMM is indeed similar to that of a CSDD and may be explained using a schematic of the CSDD with a low-profile container (Fig. 9). The sample and dialysate solutions continuously circulate through the tube at flow rate v. The solution in the tube can be divided by $N-1$ segments, so that the summation of all the segments, excluding the microchannel segment, is equal to the effective tube length [i.e., $L_t=(N-1)\cdot L$]. If all the

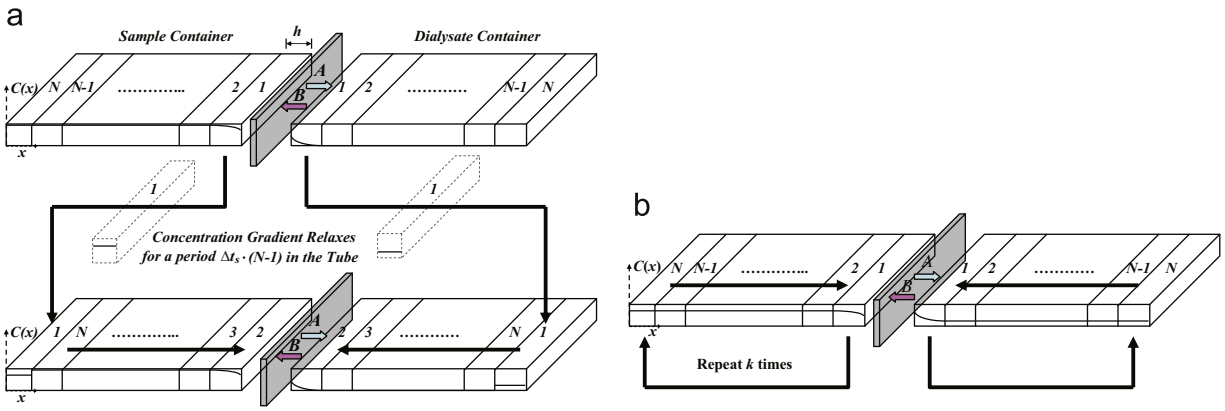

Fig. 9. The operational concept of the PDMM with recirculation tubes. (a) Bi-ionic interdiffusion proceeds between two solution segments (each from the sample and dialysate loop) and then the all segments move through the recirculation tube in First-In-First-Out manner, and (b) circulation of the segments repeats k times.

segments are stacked side-by-side in the x direction, the total length of the stack (i.e., Segment 1, 2, …, N) is equal to the length of the low-profile container ($=h\cdot N$). A segment moves inside the microchannels and the tube at flow rate v. Therefore, in effect a solution segment resides in the microchannel for $\Delta t_s(=L/v)$. During this residence time, species A and B in the first segment (Segment 1) start interdiffusing between the two microchannels through the AEM owing to concentration gradient in x direction. Flow in PDMM is laminar for the given hydrodynamic condition ($Re<335$) so we can imagine that the next segment (Segment 2) replaces Segment 1 after Δt_s, and the unstirred bi-ionic exchange begins. Meanwhile, Segment 1 left the channel and started moving along the tube for a period of $(N-1)\cdot\Delta t_s$. After the last segment (Segment N) completes interdiffusion, Segment 1 returns to the microchannel, and all the solution segments in the recirculation loop complete one cycle. The subsequent dialysis cycles of the returned segments continue. The concentration of species A and B within all the segments can be uniform after a cycle if transverse mass transfer yields effective mixing in the tubes. Mixing by transverse mass transfer is useful in that it simplifies device design since no stirrer is required. It will be experimentally verified in Section 3.3.2.3.

Solution circulation and the dialysis process for Segment 1 to N repeat k times as shown in Fig. 9b. As the dialysis cycle repeats, the average concentration of species A of the sample loop continues to decreasing and that of the dialysate loop continues to increasing until the entire solutions in both loops reach the Donnan equilibrium.

It is easy to imagine that agitation in the CSDD yields "global" mixing throughout the entire solution volume inside the container. In the PDMM, however, a series of unagitated solution segments move side-by-side inside an imaginary container in FIFO (First-In-First-Out) fashion as shown in Fig. 9a. This FIFO movement yields "sequential" mixing. Because of the global mixing, mass transfer of the CSDD should be more effective than that of the PDMM when the dimensional parameters of the imaginary container and the low-profile container are matched (i.e., container length: $X_1=X_2=h\cdot N$, and cross-sectional area: $A_m=W\cdot L$). However, as pointed out previously, effective agitation in the CSDD with the low-profile container was extremely difficult.

3.3.2.2. Advantages of the PDMM over the CSDDs. The PDMM is better for the microanalytical systems than the CSDD. The chief advantage is that the "effective length" of the container can be increased without expanding other dimensions of the container (i.e., width and height). Thus, irreproducibility can be reduced without an unacceptable volume increase. Compared to the CSDD with the low-profile container hydrodynamic condition is much better owing to the forced convection through the tubes even with the small solution volume. Unagitated bi-ionic interdiffusion in a segment can be improved if the height of the microfluidic channel h (i.e., diffusion length) decreases. Also, simply increasing flow rate can improve overall mixing efficiency up to a certain extent by replacing dialyzed solution segments faster.

3.3.2.3. Two limiting conditions for mass transfer inside a solution segment moving through the recirculation tubes. One assumption behind the operational principle of the PDMM is that concentration profile of a solution segment in the recirculation tube is uniform after a cycle is completed. Our recirculation loop does not have a stirring tank unlike Ref. [29]. Transverse mass transfer could yield effective mixing inside the tube in a proper hydrodynamic condition. There are two limiting cases: (1) transverse mass transfer within the solution segments is egligible therefore the concentration profile from the previous dialysis remains unchanged; (2) transverse mass transfer is significant so that the concentration profile in each solution segment becomes uniform (i.e., perfect mixing).

The mass transfer condition was examined experimentally using a Kenics static mixer. The dialysis experiments with an AFN membrane were performed for 30 min and 1 h with and without the static mixer at four flow rates (i.e., 0.163, 0.267, 0.378, and 0.454 ms^{-1}). We observed practically no improvement in mass transfer for all the tested flow rates over the results obtained without a mixer (see Fig. S.5 in SD). The same results were obtained from the experiment done with up to four Kenics mixers installed in series. Experiments with an ACS membrane showed similar results. Our hydrodynamic condition is close to the second limiting case. The reason for this experimental result is *not because the dialysis process is membrane-diffusion controlled*. The solution- and membrane-phase mass-transfer resistances at initial dialysis process were estimated using Velizarov et al.'s approach [29]. The membrane-phase resistance ($\sim$0.5 kmol m^{-3}) was smaller than the solution-phase resistance ($\sim$1 to $\sim$10 kmol m^{-3}). As a result, the dialysis process was a combination of membrane-phase and solution-phase mass transfer and we concluded that a solution segment was blended satisfactorily during recirculation without a mixing element.

3.3.3. Transient PDMM response

Donnan dialysis of the model bi-ionic system, 1 mmol L^{-1} $NaNO_3$ |AEM| 10 mmol L^{-1} NaF, was performed using the PDMM with recirculation tubes. The transient response is studied to characterize equilibrium time since it determines throughput of an equilibrium-dialysis module [22]. Here equilibrium time is defined as the time when the dialyzer output reaches within 5% of the ideal equilibrium value (i.e., 0.9091 mmol L^{-1}). Dialysis results for both AEMs are

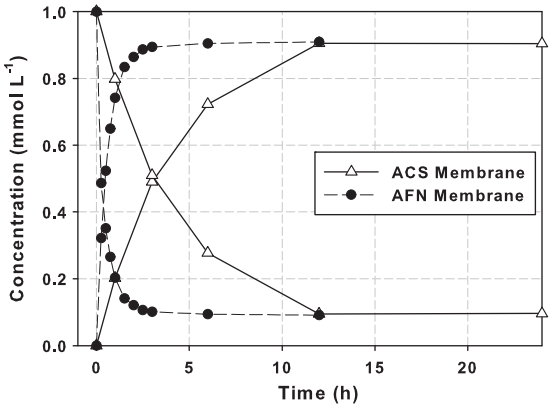

Fig. 10. Average concentration of nitrate in the entire sample and dialysate loops as a function of time.

shown in Fig. 10 (up to 12 h for the AFN and 24 h for the ACS membrane). Each data point indicates average concentration of nitrate in the entire solution loop, which is measured with the ISE. As described in Experimental section, the dialysis process was repeated for decreasing durations in order to minimize the counterion-storage effect of the AEM. If repeated for increasing duration, influence of the residual nitrate from the membrane was large for short durations (e.g., from 0.25 to 1 h) as the AEM was initially saturated with nitrate. The measured dialysate and sample nitrate concentrations were normalized such that the total nitrate concentration $C_{A,T}$ was equal to 1 mmol L^{-1} because we observed that measured $C_{A,T}$ was often higher than 1 mmol L^{-1} owing to the additional nitrate percolating from the membrane.

As seen in Fig. 10, at the flow rate of 0.163 ms^{-1} it took roughly 12 h to reach equilibrium for the ACS membrane (please note that the exact equilibrium time lies anywhere between 6 and 12 h, albeit closer to 12 h, based on our sparse *ex-situ* nitrate measurement), but 2 h for the AFN membrane. Even though the ACS membrane is thinner (123 vs. 153 μm) than the AFN membrane, the mass transport through the ACS membrane is much slower because of the highly crosslinked monovalent-ion-selective layer [40]. As a result, the throughput for the PDMM using the AFN membrane is much higher (i.e., 1 sample per 2 h). The throughput was improved up to 1 sample per 1 h by increasing the flow rate to 0.454 ms^{-1}, which may be useful for some medium-throughput applications. Flow rate for the PDMM with the ACS membrane was increased up to 0.454 ms^{-1}, but nitrate concentration at 1 h time point was not improved from the 0.163 ms^{-1} result. Thus, the ACS membrane was not useful to be used as a sample-preparation module owing to the low dialysis throughput.

Another advantage of our equilibrium-dialysis-mode PDMM is an excellent dialysis efficiency ($\sim$91%) as seen in Fig. 10. The efficiency is much higher than results of the previous parallel-plate dialyzers operating in flow-through conditions [22].

3.3.4. Improved reproducibility of the PDMM with recirculation tubes

The effective container length of the PDMM is $N \cdot h = 19.4$ cm, which is almost 8 times larger than that of the cubic CSDD container (i.e., 2.54 cm). As a result, the mass of the solution-phase counterions was also 8 times higher (i.e., 0.194 mol m^{-2} vs. 0.0254 mol m^{-2} for sample solution). Consequently, the dialyzer irreproducibility can be reduced by having a longer effective container and larger mass of ionic species than those of the CSDD. Table 2 compares dialysis performance of the three dialyzers (i.e., the CSDD with cubic containers, the CSDD with low-profile containers, and the PDMM with recirculation tubes) for the model bi-ionic system 1 mmol L^{-1} $NaNO_3$ |AEM| 10 mmol L^{-1} NaF. The number of dialysis steps required to reach within 10% error of the ideal dialyzer output was estimated by the numerical simulation. We expect that the irreproducibility of the PDMM reduces as much as 4 folds compared to the CSDD with cubic containers as can be seen in the table (AFN membrane).

3.3.5. Conductivity of the ACS and AFN membranes for various anions and the permselectivity of Donnan dialysis

Based on published data, nitrate shows higher conductivity than other anions, especially multivalent anions in the both AEMs [47]. Consequently, the estimated diffusion coefficient of nitrate is larger than the other anions of lower conductivity. Thus, in a given time, nitrate should be transferred to the dialysate solution in higher amount than other interfering anions. The ACS membrane shows even higher monovalent selectivity than the AFN membrane [40]. As a result, the ACS membrane would be beneficial for nitrate analysis [8,31] if low throughput was not an issue.

4. Conclusion

As a sample-preparation module for an analytical system, three types of Donnan dialyzers were designed, fabricated, and analyzed. Miniaturized continuous stirred-tank dialyzers (CSDD) were proposed chiefly for reduced sample consumption. The counterion-storage effect resulted in dependence of Donnan-dialysis process on the prior dialyzer state, causing nonlinear and irreproducible dialyzer output of the CSDD with cubic containers. The theoretical analysis and experimental results evidenced such dependency of Donnan dialyzers. Our analysis provides a useful guideline for dialyzer design. It was suggested to use a large solution-to-membrane volume ratio R_V for better reproducibility. The CSDD with low-profile containers would show better reproducibility but dialysis process was too slow to be practical owing to ineffective mixing in the scaled-down container.

We proposed an elegant solution to the CSDD problems by replacing the container with micro-bore tube and using a micro-fluidic parallel-plate dialyzer unit. R_V was improved by having the long tubes as containers. Reproducibility was improved by a factor of 4, compared with a CSDD with cubic containers (AFN membrane). Dialysis was fast owing to forced convection even without a mixing element. Throughput was improved about 6 fold compared with that of the low-profile CSDD (ACS membrane). One could improve the throughput of the PDMM further by forcing solutions at higher flow rates. A thinner membrane with smaller exchange capacity than the AEMs used here could be employed for even less irreproducibility and faster dialysis.

The proposed dialyzer could be an effective membrane separation module for a miniaturized total analysis system. Currently our PDMM device uses 10 mL solution volume. However, theoretically the volume can be much less if a smaller membrane piece and a tube of smaller diameter are used. The PDMM operates in equilibrium condition, and thus dialysis efficiency is close to 91%. Thus, analytical-signal loss can be minimal compared to a non-equilibrium flow-through dialyzer where the dialysis efficiency is usually about 1%. Using the tube as a container, interfacing with a miniaturized total analysis system should be straightforward. We also demonstrated automated sample loading and dialysis using the computer-controlled peristaltic pump and the custom multi-channel valve manifold.

Lastly, a “dialyzer-on-a-chip” based on our PDMM concept could be realized without much difficulty as the PDMM would readily scale down. A recirculation tube could be fabricated on a polymer or a glass substrate as a serpentine microfluidic channel. A channel height, thinner than one used here, could lead to

a higher throughput (i.e., shorter diffusion length) and it could be easily realized using routine microfabrication techniques.

Acknowledgments

We would like to gratefully acknowledge that our research was funded by the NSF and the Center for Embedded Network Sensing at UCLA (NSF CCR-0120778). This work was also supported by 2013 Research Fund of Myongji University. We want to give a tribute to Dr. Ira B. Goldberg (deceased) for his excellent and insightful discussion on the theoretical aspect of this research.

Appendix A. Supplementary data

Supplementary data associated with this article can be found in the online version at http://dx.doi.org/10.1016/j.memsci.2014.02.029.

References

[1] S.C. Terry, J.H. Jerman, J.B. Angell, A gas chromatographic air analyzer fabricated on a silicon wafer, IEEE Trans. Electron. Dev. 26 (1979) 1880–1886.
[2] G.M. Whitesides, The origins and the future of microfluidics, Nature 442 (2006) 368–373.
[3] C.D. Chin, V. Linder, S.K. Sia, Commercialization of microfluidic point-of-care diagnostic devices, Lab Chip 12 (2012) 2118–2134.
[4] L. Bousse, S. Mouradian, A. Minalla, H. Yee, K. Williams, R. Dubrow, Protein sizing on a microchip, Anal. Chem. 73 (2001) 1207–1212.
[5] A.J. de Mello, N. Beard, Focus dealing with 'real' samples: sample pre-treatment in microfluidic systems, Lab Chip 3 (2003) 11N–20N.
[6] R. Mariella, Sample preparation: the weak link in microfluidics-based biodetection, Biomed. Microdev. 10 (2008) 777–784.
[7] J. Lichtenberg, N.F. de Rooij, E. Verpoorte, Sample pretreatment on microfabricated devices, Talanta 56 (2002) 233–266.
[8] D. Kim, I.B. Goldberg, J.W. Judy, Microfabricated electrochemical nitrate sensor using double-potential-step chronocoulometry, Sensor Actuat. B-Chem. 135 (2009) 618–624.
[9] D. Kim, K. Karns, S.Q. Tia, M. He, A.E. Herr, Electrostatic protein immobilization using charged polyacrylamide gels and cationic detergent microfluidic western blotting, Anal. Chem. 84 (2012) 2533–2540.
[10] L.A. Legendre, J.M. Bienvenue, M.G. Roper, J.P. Ferrance, J.P. Landers, A simple, valveless microfluidic sample preparation device for extraction and amplification of dna from nanoliter-volume samples, Anal. Chem. 78 (2006) 1444–1451.
[11] K.P. Nichols, R.R. Pompano, L. Li, A.V. Gelis, R.F. Ismagilov, Toward mechanistic understanding of nuclear reprocessing chemistries by quantifying lanthanide solvent extraction kinetics via microfluidics with constant interfacial area and rapid mixing, J. Am. Chem. Soc. 133 (2011) 15721–15729.
[12] M.J. Jebrail, A.R. Wheeler, Digital microfluidic method for protein extraction by precipitation, Anal. Chem. 81 (2008) 330–335.
[13] P. Jandik, B. Weigl, N. Kessler, J. Cheng, C. Morris, T. Schulte, N. Avdalovic, Initial study of using a laminar fluid diffusion interface for sample preparation in high-performance liquid chromatography, J. Chromatogr. A 954 (2002) 33–40.
[14] J. de Jong, R. Lammertink, M. Wessling, Membranes and microfluidics: a review, Lab Chip 6 (2006) 1125–1139.
[15] J. Ou, T. Glawdel, R. Samy, S. Wang, Z. Liu, C.L. Ren, J. Pawliszyn, Integration of dialysis membranes into a poly (dimethylsiloxane) microfluidic chip for isoelectric focusing of proteins using whole-channel imaging detection, Anal. Chem. 80 (2008) 7401–7407.
[16] M. Miró, W. Frenzel, Automated membrane-based sampling and sample preparation exploiting flow-injection analysis, Trends Anal. Chem. 23 (2004) 624–636.
[17] D. Turnell, J. Cooper, Automated preparation of biological samples prior to high pressure liquid chromatography: part I-the use of dialysis for deproteinizing serum for amino-acid analysis, J. Auto. Chem. 7 (1985) 177–180.
[18] M. Miró, W. Frenzel, The potential of microdialysis as an automatic sample-processing technique for environmental research, Trends Anal. Chem. 24 (2005) 324–333.
[19] S. Song, A.K. Singh, T.J. Shepodd, B.J. Kirby, Microchip dialysis of proteins using in situ photopatterned nanoporous polymer membranes, Anal. Chem. 76 (2004) 2367–2373.
[20] Y. Jiang, P.-C. Wang, L.E. Locascio, C.S. Lee, Integrated plastic microfluidic devices with ESI-MS for drug screening and residue analysis, Anal. Chem. 73 (2001) 2048–2053.
[21] J.F. van Staden, Review: membrane separation in flow infection systems, part 1: dialysis, Fresen. J. Anal. Chem. 352 (1995) 271–302.
[22] M. de Castro, F.P. Capote, N.S. Ávila, Is dialysis alive as a membrane-based separation technique? Trends Anal. Chem. 27 (2008) 315–326.
[23] W. Blaedel, T. Kissel, Chemical enrichment and exclusion with ion exchange membranes, Anal. Chem. 44 (1972) 2109–2111.
[24] S. Rosario, G. Sig Cha, M. Meyerhoff, M. Trojanowicz, Use of ionomer membranes to enhance the selectivity of electrode-based biosensors in flow-injection analysis, Anal. Chem. 62 (1990) 2418–2424.
[25] T.M. Squires, S.R. Quake, Microfluidics: fluid physics at the nanoliter scale, Rev. Mod. Phys. 77 (2005) 977.
[26] J. Koropchak, L. Allen, Flow-injection Donnan dialysis preconcentration of cations for flame atomic absorption spectrophotometry, Anal. Chem. 61 (1989) 1410–1414.
[27] J.A. Cox, Z. Twardowski, Tubular flow donnan dialysis, Anal. Chem. 52 (1980) 1503–1505.
[28] J. Cox, G. Litwinski, High sample convection Donnan dialysis, Anal. Chem. 55 (1983) 1640–1642.
[29] S. Velizarov, M.A. Reis, J.G. Crespo, Removal of trace mono-valent inorganic pollutants in an ion exchange membrane bioreactor: analysis of transport rate in a denitrification process, J. Membr. Sci. 217 (2003) 269–284.
[30] E. Milosavljevic, L. Solujic, J. Hendrix, J. Nelson, Flow injection gas-diffusion method for preconcentration and determination of trace sulfide, Anal. Chem. 60 (1988) 2791–2796.
[31] D. Kim, I.B. Goldberg, J.W. Judy, Chronocoulometric determination of nitrate on silver electrode and sodium hydroxide electrolyte, Analyst 132 (2007) 350–357.
[32] H. Miyoshi, M. Chubachi, M. Yamagami, T. Kataoka, Characteristic coefficients for equilibrium between solution and Neosepta or Selemion cation exchange membranes, J. Chem. Eng. Data 37 (1992) 120–124.
[33] D.S. Jan, C.C. Ho, F.N. Tsai, Combined film and membrane diffusion-controlled transport of ions through charged membrane, J. Membr. Sci. 90 (1994) 109–116.
[34] K. Sato, T. Yonemoto, T. Tadaki, The determination of diffusion coefficients of counter-ions in the ion-exchange membrane by means of batchwise Donnan dialytic experiments, J. Membr. Sci. 53 (1990) 215–227.
[35] F.G. Helfferich, Ion Exchange, McGraw-Hill, Inc., New York, 1962.
[36] T. Sata, Studies on anion exchange membranes having permselectivity for specific anions in electrodialysis – effect of hydrophilicity of anion exchange membranes on permselectivity of anions, J. Membr. Sci. 167 (2000) 1–31.
[37] E. Güler, W. van Baak, M. Saakes, K. Nijmeijer, Monovalent-ion-selective membranes for reverse electrodialysis, J. Membr. Sci, 455 (2014) 254-270.
[38] Z. Palaty`, A. Žáková, Apparent diffusivity of some inorganic acids in anion-exchange membrane, J. Membr. Sci. 173 (2000) 211–223.
[39] D.A. Clifford, Ion exchange and inorganic adsorption, in: American Water Works Association (Ed.), Water Quality & Treatment: A Handbook on Drinking Water, McGraw-Hill, New York, 2011, pp. 9.1–9.91.
[40] G. Saracco, Transport properties of monovalent-ion-permselective membranes, Chem. Eng. Sci. 52 (1997) 3019–3031.
[41] H. Strathmann, Ion-exchange Membrane Separation Processes, Elsevier Science, Boston, 2004.
[42] B. Bernhardsson, E. Martins, G. Johansson, Solute transfer in on-line analytical flow-through dialyzers, Anal. Chim. Acta 167 (1985) 111–122.
[43] S.D. Kolev, W.E. van der Linden, Analysis of transient laminar mass transfer in a parallel-plate dialyser, Anal. Chim. Acta 257 (1992) 331–342.
[44] V.M. Starov, D.N. Petsev, I.B. Ivanov, Diffusion model of Donnan dialysis under flow conditions, J. Membr. Sci. 53 (1990) 45–57.
[45] H.-M. Yeh, Analysis of dialysis in cross-flow parallel-plate membrane modules with feed-stream recycle for improved performance, Chem. Eng. Commun. 197 (2009) 455–465.
[46] D. Kim, Micromachined chronocoulometric nitrate sensor and parallel-plate Donnan-Dialytic sample-preparation system using anion-exchange membrane (Ph.D. thesis), University of California, Los Angeles, CA, USA, 2008.
[47] N. Pismenskaya, V. Nikonenko, B. Auclair, G. Pourcelly, Transport of weak-electrolyte anions through anion exchange membranes: current–voltage characteristics, J. Membr. Sci. 189 (2001) 129–140.